



Quantitative morphometric analysis of hepatocellular carcinoma: development of a programmed algorithm and preliminary application

Felix Y. Yap, James T. Bui, M. Grace Knuttinen, Natasha M. Walzer, Scott J. Cotler, Charles A. Owens, Jamie L. Berkes, Ron C. Gaba

PURPOSE

The quantitative relationship between tumor morphology and malignant potential has not been explored in liver tumors. We designed a computer algorithm to analyze shape features of hepatocellular carcinoma (HCC) and tested feasibility of morphologic analysis.

MATERIALS AND METHODS

Cross-sectional images from 118 patients diagnosed with HCC between 2007 and 2010 were extracted at the widest index tumor diameter. The tumor margins were outlined, and point coordinates were input into a MATLAB (MathWorks Inc., Natick, Massachusetts, USA) algorithm. Twelve shape descriptors were calculated per tumor: the compactness, the mean radial distance (MRD), the RD standard deviation (RDS), the RD area ratio (RDAR), the zero crossings, entropy, the mean Feret diameter (MFD), the Feret ratio, the convex hull area (CHA) and perimeter (CHP) ratios, the elliptic compactness (EC), and the elliptic irregularity (EI). The parameters were correlated with the levels of alpha-fetoprotein (AFP) as an indicator of tumor aggressiveness.

RESULTS

The quantitative morphometric analysis was technically successful in all cases. The mean parameters were as follows: compactness 0.88 ± 0.086 , MRD 0.83 ± 0.056 , RDS 0.087 ± 0.037 , RDAR 0.045 ± 0.023 , zero crossings 6 ± 2.2 , entropy 1.43 ± 0.16 , MFD 4.40 ± 3.14 cm, Feret ratio 0.78 ± 0.089 , CHA 0.98 ± 0.027 , CHP 0.98 ± 0.030 , EC 0.95 ± 0.043 , and EI 0.95 ± 0.023 . MFD and RDAR provided the widest value range for the best shape discrimination. The larger tumors were less compact, more concave, and less ellipsoid than the smaller tumors ($P < 0.0001$). AFP-producing tumors displayed greater morphologic irregularity based on several parameters, including compactness, MRD, RDS, RDAR, entropy, and EI ($P < 0.05$ for all).

CONCLUSION

Computerized HCC image analysis using shape descriptors is technically feasible. Aggressively growing tumors have wider diameters and more irregular margins. Future studies will determine further clinical applications for this morphologic analysis.

The relationship between tumor morphology on diagnostic imaging and assessment of malignancy potential has been explored in a variety of cancers (1–3). Benign lung and breast tumors usually have compact shapes and well-defined margins, whereas malignant cancers are more irregular and lobulated (4, 5). Numerous shape descriptors exist in the literature; each descriptor focuses on particular characteristics of tumor morphology and factors them into a quantitative calculation. One such factor, compactness, has been used to characterize the contours of breast (6), lung (7), oral squamous cell (1), and renal cell carcinomas (3) as a malignancy marker or an indicator of tumor aggression. Mammography, in particular, exploits the qualitative visual relationships to distinguish benign tumors from malignant breast masses based on their radiographic appearances (4). The image analysis of breast tumors using shape descriptors has spearheaded recent development of computer-aided diagnosis (CAD) algorithms that seek to improve the diagnostic capabilities of radiologists (8). Similar CAD systems have also been explored for other neoplasms, such as thyroid nodules (9) and soft-tissue tumors (10); however, these systems have not been extensively applied to liver tumors.

Hepatocellular carcinoma (HCC) is the most common primary hepatic malignancy and the third leading cause of cancer-related deaths worldwide (11–14). HCC may manifest a variety of gross morphologies, including nodular, nodular with perinodular extension, multinodular confluent, and infiltrative types (15); each morphology is associated with different degrees of malignancy and variable clinical outcomes (16–18). While some HCC shapes, such as focal nodular varieties, have been associated with more favorable prognoses (19), other HCC morphologies, such as infiltrative and multinodular confluent forms, have been linked to poor patient survival (20, 21). Current HCC morphologic imaging assessment is limited to subjective and qualitative descriptions, which may be confounded by inter-observer variation and lack the measurable parameters that allow reproducible tumor morphologic descriptions, numerical comparisons of tumor shapes, and the association of tumor contour descriptors with clinical outcomes. Truly objective and quantitative metrics to describe HCC morphology may improve the understanding of tumor natural history and treatment response prediction.

This study was thus undertaken with the purpose of designing a computer algorithm with an extensive array of shape descriptors to quantitatively evaluate HCC imaging contours in an efficient fashion, thereby testing the feasibility of HCC tumor morphologic analysis and correlating these morphologic parameters to the alpha-fetoprotein (AFP) levels, which are an accepted indicator of tumor aggression.

From the Departments of Radiology (F.Y.Y., G.K., C.A.O., R.C.G. ✉ rongaba@yahoo.com), and Hepatology (J.T.B., N.M.W., S.J.C., J.L.B.), University of Illinois at Chicago, Chicago, Illinois, USA.

Received 23 April 2012; revision requested 12 June 2012; revision received 18 June 2012; Accepted 9 July 2012.

Published online 30 November 2012
DOI 10.4261/1305-3825.DIR.5973-12.1

Materials and methods

This study was in compliance with the Health Insurance Portability and Accountability Act, and the institutional review board at our institution granted approval with consent waivers for inclusion in the study.

Patients and tumors

Imaging studies of 165 consecutive patients with HCC were reviewed at our institutional multidisciplinary liver cancer management conferences between 2007 and 2010. HCC in these patients was diagnosed by percutaneous biopsy or noninvasively based on the presence of a hepatic mass larger than 2 cm in diameter with characteristic imaging findings (22) of arterial phase contrast enhancement and portal venous phase washout. The inclusion criteria consisted of a diagnosis of HCC limited to T0-T4, M0 stage disease, and the availability of baseline imaging using multiphase helical computed tomography (CT) or dynamic magnetic resonance imaging (MRI). The lack of accessible baseline imaging and M1 stage HCC were exclusion criteria.

Image acquisition

The CT studies were obtained with a triple phase protocol on a LightSpeed VCT scanner (GE Healthcare, Pewaukee, Wisconsin, USA) after intravenous injection of 150 mL iohexol (Omnipaque-300, Amersham Health, Princeton, New Jersey, USA). The acquisition parameters included 2.5-mm collimation, 2.5-mm reconstruction interval, and 0.984:1 pitch. The MRI was performed with a 1.5 Tesla (T) system (Signa EXCITE 1.5T, GE Healthcare) with an eight-channel body coil. The gadolinium-enhanced dynamic imaging was acquired by three-dimensional (3D) gradient-echo sequences (LAVA, GE Healthcare) after the intravenous administration of 0.2 mL/kg of gadodiamide (Omniscan, GE Healthcare) or 0.1 mL/kg of Gadoxetate disodium (Eovist, Bayer HealthCare Pharmaceuticals, Montville, New Jersey, USA). The acquisition parameters included TR 4.0–4.3 ms, TE 2.0 ms, flip angle 12°, matrix 320×192, slice thickness 5 mm, and slice gap 2.5 mm.

Tumor contour extraction

Two independent operators evaluated the baseline tumor cross-section-

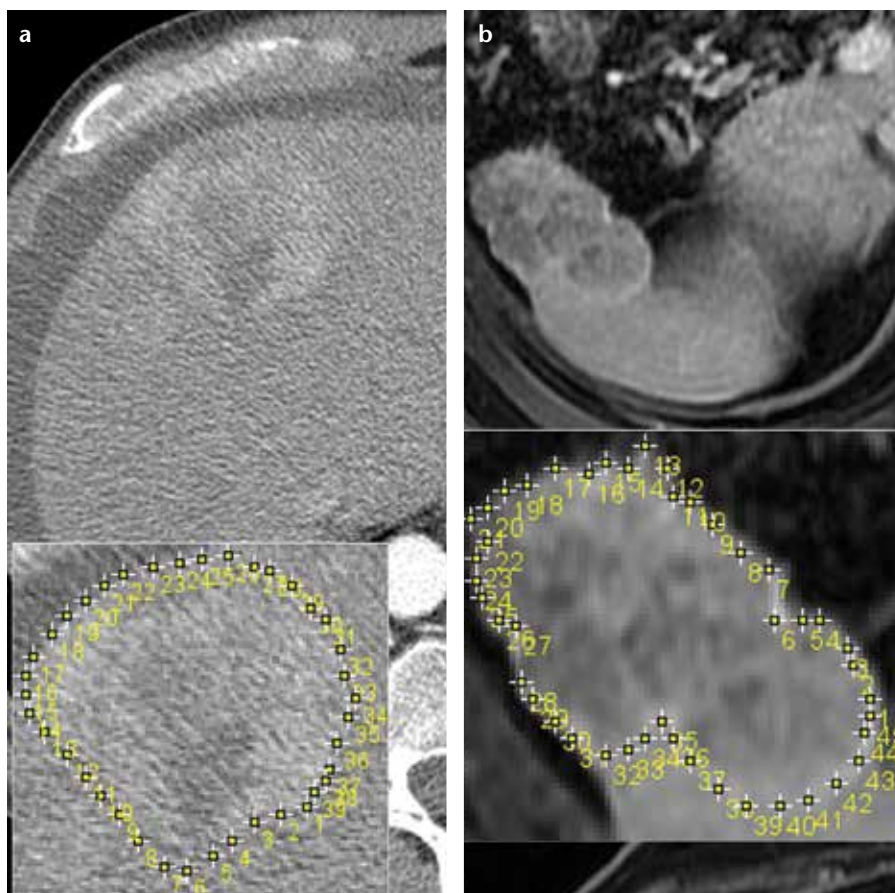


Figure 1. a, b. Examples of the HCC index tumors at their maximum transverse diameters with respective tumor margin outlines (insets). Tumor 1 (a) was found in a 62-year-old Caucasian man with alcoholic cirrhosis and was diagnosed by imaging. Boundary sampling with 39 points; tumor area=31 cm², tumor perimeter=20.6 cm, compactness=0.92. Tumor 2 (b) was found in an 86-year-old Hispanic man with alcoholic cirrhosis and was confirmed by biopsy. Boundary sampling with 45 points; tumor area=13.3 cm², tumor perimeter=15.8 cm, compactness=0.67.

al imaging and categorized the tumor enhancement pattern as either typical (arterial enhancement followed by contrast washout in delayed phases) or atypical. The final tumor classification was made by consensus decision. A radiologist with nine years of experience then extracted arterial phase images at the representative axial slice using the widest possible tumor diameter (Fig. 1). For the analysis of multiple tumors, we selected the largest dominant first-treated lesion, which was identified as the “primary index tumor” (23). The tumor margins were sampled using the ImageJ software multipoint tool, and a computerized linear interpolation using MATLAB (MathWorks Inc., Natick, Massachusetts, USA) connected the sample points with additional boundary points to form a more complete border. Using this interpolation step, two radiologists could outline

the tumor boundary differently and still produce two final coordinate sets of similar, if not equal, lengths, hence reducing inter-observer variability. The aspect ratio of each image was used to convert the units for length and area from pixels to cm and cm².

Tumor shape analysis and feature extraction

Each set of coordinates was input into MATLAB, which calculated the area, perimeter, and 12 shape features for each tumor. The selected shape descriptors have been studied in CAD algorithms for various cancers (1–3, 6–10, 24) and share the important property of independence from shape resizing, translation, and rotation.

Tumor shape descriptors

Brief descriptions of each shape descriptor are presented in Table 1, and

more detailed descriptions and equations for each shape descriptor may be found in the Appendix.

Qualitative and statistical analysis

The MATLAB algorithm superimposed the tumor convex hull and fitting ellipse onto each tumor contour. To confirm the validity of the algorithm, we reviewed and compared these composite images to the original radiologic images. The morphometric parameters of different tumor sizes were compared using an analysis of variance. The parameters between pairs of tumor cohorts were compared using Student's *t* test. A correlation matrix of shape features was constructed using Microsoft Excel 2010 software (Microsoft Inc., Redmond, Washington, USA). The parameters of the AFP producing tumors and the nonproducing tumors were compared to test the hypothesis that more aggressive tumors (as manifested by greater AFP production) have quantitative parameters that are reflective of greater morphologic irregularity. The statistical analysis was performed using a commercially available software (Statistical Package for Social Sciences, version 18, SPSS Inc., Chicago, Illinois, USA).

Results

Patients and tumors

Our final patient cohort included 118 (72%) of the 165 HCC patients. The 118 patients had undergone multiphase helical CT or dynamic contrast-enhanced MRI between 2007 and 2010 for diagnosis and/or staging of HCC. Twenty-eight (17%) of the original 165 patients were excluded from the final cohort because of unavailable imaging from outside hospitals, and six (4%) were excluded due to the lack of multiphase contrast-enhanced imaging studies. An additional 13 patients (8%) were excluded due to advanced disease. The final study cohort included 95 males (81%) and 23 females (19%), and the mean patient age was 61 ± 10 years (age range, 26–87 years). CT scans were performed on 86 (73%) of 118 patients, and 32 (27%) of 118 patients underwent MRI. In 68 patients (58%), HCC was diagnosed by imaging alone. In the remaining 50 patients (42%), HCC was confirmed through biopsy. The histologic grade was provided for 44 of 52 biopsied tumors; 16 tumors were graded as

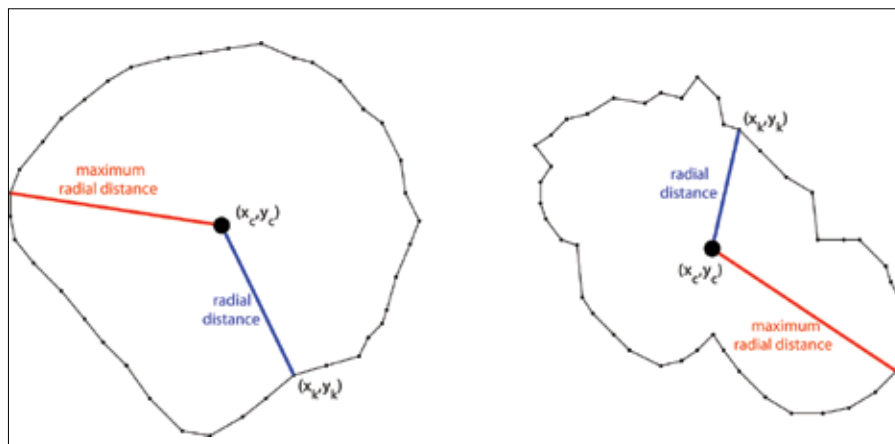


Figure 2. Each tumor is shown with the radial distance (RD) defined as the Euclidean distance from the centroid (x_c, y_c) to the boundary point (x_k, y_k) . All of the RD are normalized to a maximum radial distance (*red*), and the length is defined as 1. In this case, Tumor 1 mean RD (MRD) is 0.88 and RD standard deviation (RDS) is 0.057, while Tumor 2 MRD is 0.72 and RDS is 0.169.

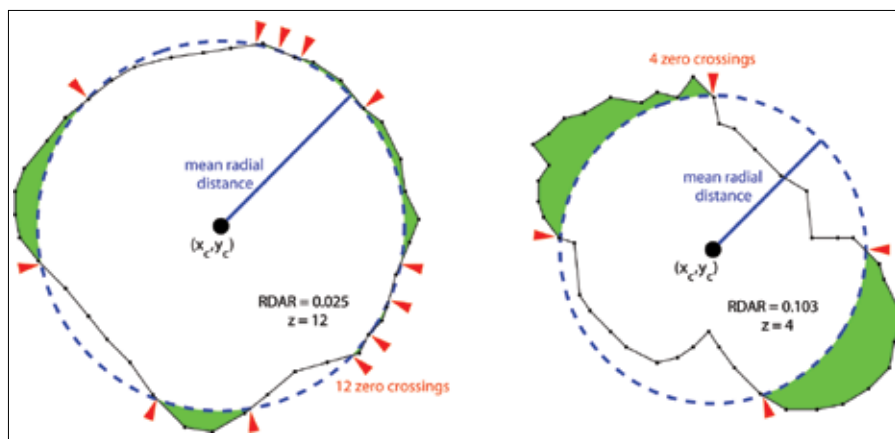


Figure 3. The radial distance area ratio (RDAR) indicates the degree to which a tumor extends outside the equivalent circle centered at centroid (x_c, y_c) with a radius equal to the MRD. Zero crossing count (*z*) indicates how frequently the tumor contour crosses the equivalent circle (*red arrow heads*).

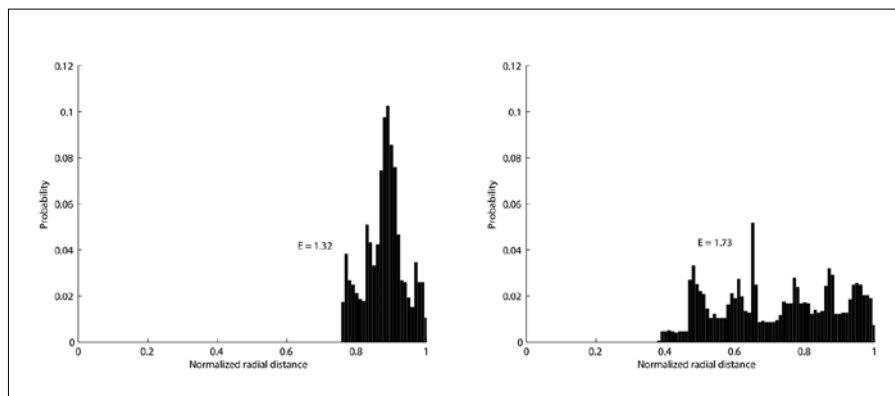


Figure 4. Histograms showing the distribution of radial distances. The entropy estimator (*E*) is calculated from the histogram.

well-differentiated, 21 as moderately differentiated, and seven as poorly differentiated. The mean index tumor diameter was 4.6 ± 3.6 cm (range, 1–23 cm). Twenty-five percent (29 of 118) of the index tumors were located in the

left hepatic lobe, and 89 (75%) of 118 index tumors were located in the right hepatic lobe. Solitary tumors were found in 65 (55%) of 118 patients, whereas 53 (45%) of 118 patients had multifocal disease. The serum AFP

Table 1. Brief descriptions of shape features and their value ranges

Shape feature	Brief description	Minimum value	Maximum value
Compactness (Fig. 1)	How well boundary encloses largest possible area for perimeter	0	1 (for a circle)
Mean radial distance (Fig. 2)	Mean of all radial distances	0	1 (for a circle)
Standard deviation of the radial distance (Fig. 2)	Standard deviation of all radial distances	0 (for a circle)	1
Radial distance area ratio (Fig. 3)	How much tumor extends outside equivalent circle centered on tumor with radius equal to mean radial distance	0	1 (for a circle)
Zero crossing count (z) (Fig. 3)	How often tumor contour crosses its equivalent circle	0	Approaches ∞ (for a meandering, lobulated contour)
Histogram estimator of entropy (Fig. 4)	Probabilistic measure of variability in tumor radial distances	Approaches 0 (for a compact tumor)	Approaches ∞ (for an irregular tumor)
Feret ratio (Fig. 5)	Ratio of minimum Feret diameter to maximum Feret diameter	0	1 (for a circle)
Mean Feret diameter (Fig. 5)	Mean of all Feret diameters from all orientations	Size dependent	Size dependent
Convex hull area ratio (Fig. 6)	Measure of tumor convexity	0	1 (for a convex shape without concavities)
Convex hull perimeter ratio (Fig. 6)	Measure of tumor convexity	0	1 (for a convex shape without concavities)
Elliptic compactness (Fig. 7)	How closely tumor resembles ellipsoid	0	1 (for an ellipse)
Elliptic irregularity (Fig. 7)	How closely tumor resembles ellipsoid	0	1 (for an ellipse)

value was not available for three patients at the time of diagnosis.

Tumor morphometric analysis

Computed tumor morphometric analysis and shape descriptor calculation was technically successful in all cases (Table 2). Mean number of sample points was 30 ± 14 (range, 13–83) for each tumor. The total execution time for the MATLAB algorithm for all 118 tumors was 59 s. A postimage analysis comparison of the composite images to the radiologic images yielded no major discrepancies; therefore, we confirmed that our algorithm accurately performed its mathematical analysis.

The mean tumor areas and perimeters were 20.5 ± 34.4 cm² (range, 0.8–284 cm²) and 14.2 ± 10.6 cm (range, 3.3–65.6 cm), showing a wide variation in tumor sizes. Of the 12 shape-based descriptors analyzed, three had the widest dispersion in their distributions according to their coefficients of variations (CV): mean Feret diameter (MFD) (CV=0.71), the radial distance area ratio (RDAR) (CV=0.51), and the radial distance standard deviation (RDSD) (CV=0.42). This dispersion suggests that MFD, RDAR, and RDSD may best allow for the discrimination of tu-

Table 2. Measurement of tumor area and perimeter, and shape features of 118 HCC tumors

Shape descriptor	Mean	Range	SD	CV
Tumor area (cm ²)	20.5	0.8–284	34.4	1.68
Tumor perimeter (cm)	14.2	3.3–65.6	10.6	0.75
Compactness	0.88	0.52–0.98	0.086	0.097
Mean RD	0.83	0.64–0.93	0.056	0.067
RD standard deviation	0.087	0.022–0.210	0.037	0.42
RD area ratio	0.045	0.009–0.136	0.023	0.51
Number of zero crossings	6	4–16	2.2	0.37
Entropy	1.43	0.95–1.82	0.16	0.11
MFD (cm)	4.40	1.06–20.3	3.14	0.71
Feret ratio	0.78	0.50–0.93	0.089	0.11
Convex hull area ratio	0.98	0.86–1.0	0.027	0.027
Convex hull perimeter ratio	0.98	0.83–1.0	0.030	0.031
Elliptic compactness	0.95	0.75–0.99	0.043	0.045
Elliptic irregularity	0.95	0.84–0.99	0.023	0.025

CV, coefficient of variation; HCC, hepatocellular carcinoma; RD, radial distance; SD, standard deviation; MFD, mean Feret diameter.

mor shapes. However, the convex hull area (CHA) and perimeter (CHP) ratios, the elliptic compactness (EC), and the elliptic irregularity (EI) are less useful because the majority of their values

were too close to 1 (the value expected for a perfect ellipse) and too narrowly distributed (CV ≤ 0.045) to show major differences in tumor morphology by themselves.

Table 3. Correlation matrix between shape descriptors

	A	P	MFD	z	C	MRD	RDS	RDAR	E ^a	FR	CHA	CHP	EC
A													
P	0.93												
MFD	0.93	1.00											
z	-0.07	-0.11	-0.10										
C	-0.30	-0.41	-0.35	0.17									
MRD	-0.16	-0.21	-0.17	0.42	0.79								
RDS	0.20	0.30	0.26	-0.52	-0.83	-0.88							
RDAR	0.20	0.31	0.27	-0.52	-0.83	-0.90	0.99						
E ^a	0.17	0.27	0.23	-0.48	-0.84	-0.90	0.97	0.95					
FR	-0.07	-0.12	-0.10	0.56	0.57	0.84	-0.83	-0.87	-0.82				
CHA	-0.23	-0.33	-0.29	0.07	0.90	0.62	-0.68	-0.66	-0.70	0.42			
CHP	-0.41	-0.55	-0.48	0.08	0.89	0.52	-0.62	-0.61	-0.60	0.30	0.77		
EC	-0.34	-0.46	-0.39	0.04	0.95	0.61	-0.66	-0.64	-0.67	0.32	0.86	0.96	
EI	-0.23	-0.33	-0.28	0.15	0.86	0.68	-0.74	-0.70	-0.75	0.34	0.79	0.74	0.85

A, area; C, compactness; CHA, convex hull area ratio; CHP, convex hull area perimeter; E, entropy of radial distance; EC, elliptic compactness; EI, elliptic irregularity; FR, Feret ratio MFD, mean Feret diameter; z, zero crossing count; MRD, mean radial distance; P, perimeter; RDAR, radial distance area ratio; RDS, radial distance standard deviation.

^aLogarithmic regression.

Table 3 shows the correlations between the shape descriptors, which were performed to elucidate any inter-relationships between the shape metrics and to determine which of these parameters might be interchangeable. Two distinct clusters emerged in which the descriptors exhibited very strong correlations with one another: (1) compactness, mean radial distance (MRD), RDS, RDAR, and entropy ($r > 0.83$ or $r < -0.83$); and (2) compactness, CHA, CHP, EC, and EI ($r \geq 0.74$). In contrast, the three size-dependent descriptors (tumor area and perimeter, MFD) were noted to correlate poorly with all of the size-independent shape features ($-0.55 \leq r \leq 0.31$), implying that the shape of a tumor is distinct from its size.

Table 4 shows the results of comparative analysis of tumor shape features between different tumor size categories. Significant differences were found between the smaller and larger tumors for size-dependent features as well as a handful of size-independent measures (particularly compactness, RDS, RDAR, CHP, and EC [$P \leq 0.003$ for all]). This finding confirms that these mathematical parameters can be used to stratify tumors by their index diameters and also implies that larger tumors collectively tend to be less compact, more concave, and less ellipsoid.

Table 4. Comparison of tumor shape features according to HCC size (mean values)

Shape descriptor	HCC <3 cm (n=50)	HCC 3–7 cm (n=46)	HCC >7 cm (n=22)	P
Tumor area (cm ²)	3.8	15.0	70.4	< 0.0001
Tumor perimeter (cm)	6.8	14.0	31.7	< 0.0001
Compactness	0.90	0.89	0.82	< 0.0001
Mean RD	0.84	0.84	0.81	0.061
RD standard deviation	0.078	0.086	0.110	0.003
RD area ratio	0.040	0.044	0.060	0.002
Number of zero crossings	6.4	6.1	5.4	0.215
Entropy	1.40	1.41	1.52	0.011
MFD (cm)	2.15	4.39	9.54	< 0.0001
Feret ratio	0.80	0.78	0.75	0.181
Convex hull area ratio	0.98	0.97	0.96	0.003
Convex hull perimeter ratio	0.99	0.99	0.96	< 0.0001
Elliptic compactness	0.96	0.96	0.92	< 0.0001
Elliptic irregularity	0.96	0.96	0.94	0.003

HCC, hepatocellular carcinoma; RD, radial distance; MFD, mean Feret diameter.

The tumor marker elevation was significantly increased in the AFP producing tumors (116 068.9 vs. 33.6 ng/mL, $P < 0.0001$) (Table 5). A comparative analysis showed that AFP producing tumors displayed more morphologic irregularity than nonproducing tumors and also had larger diameters (6.1 vs. 3.8 cm, $P = 0.004$), less compactness (0.854 vs. 0.894, $P = 0.033$), smaller MRDs (0.815 vs. 0.838, $P = 0.045$), greater RDS (0.098 vs. 0.083, $P = 0.038$), greater RDAR (0.053 vs. 0.042, $P = 0.027$), and greater entropy

Table 5. Comparison of AFP values, enhancement patterns, and tumor shape features between AFP-producing and nonproducing HCC

Parameter	AFP-producing HCC (n=31)	AFP-nonproducing HCC (n=84)	P
AFP (ng/mL)	116.068.9	33.6	< 0.0001
Enhancement pattern			
Typical	23/31 (74%)	56/84 (67%)	0.457
Atypical	8/31 (26%)	28/84 (33%)	0.457
Shape descriptors			
Tumor area (cm ²)	39.0±56.3	14.2±18.7	0.011
Tumor perimeter (cm)	20.2±15.1	12.2±7.6	0.004
Compactness	0.854±0.110	0.894±0.074	0.033
Mean RD	0.815±0.068	0.838±0.050	0.045
RD standard deviation	0.098±0.043	0.083±0.034	0.038
RD area ratio	0.053±0.029	0.042±0.020	0.027
Number of zero crossings	5.9±2.2	6.1±2.28	0.720
Entropy	1.47±0.18	1.41±0.16	0.042
MFD (cm)	6.14±4.44	3.81±2.29	0.004
Feret ratio	0.762±0.109	0.790±0.081	0.102
Convex hull area ratio	0.971±0.031	0.978±0.025	0.145
Convex hull perimeter ratio	0.974±0.043	0.988±0.024	0.046
Elliptic compactness	0.942±0.056	0.958±0.037	0.071
Elliptic irregularity	0.946±0.027	0.956±0.021	0.043

AFP, alpha-fetoprotein; HCC, hepatocellular carcinoma; RD, radial distance; MFD, mean Feret diameter. Data are given as mean±SD or n (%).

(1.47 vs. 1.41, $P = 0.042$). In addition, AFP producing tumors were more concave (CHP 0.974 vs. 0.988, $P = 0.046$) and less ellipsoid (EI 0.946 vs. 0.956, $P = 0.043$) than their less aggressive counterparts. There was no difference in the enhancement pattern between AFP producing and nonproducing tumors (56 of 84, 67% typical vs. 23 of 31, 74% typical; $P = 0.457$).

A comparative analysis of the biopsy-proven HCC tumors and those diagnosed noninvasively demonstrate that tumors selected for biopsy tend to produce less AFP, demonstrate atypical vascular patterns on imaging, and also have generally more compact and rounder borders (Table 6). The biopsied tumors had significantly greater compactness (0.898 vs. 0.871, $P = 0.037$) and MRDs (0.841 vs. 0.824, $P = 0.045$) and greater EC (0.961 vs. 0.948, $P = 0.047$). In addition, a greater proportion of the biopsied tumors displayed atypical enhancement patterns (22 of 50 [44%] vs. 16 of 68 [24%], $P = 0.011$).

Patients who underwent biopsy had lower AFP levels on average (736 vs. 52 567 ng/mL, $P = 0.131$) with only 8% (4/50) having AFP levels above a 400 ng/mL threshold (21 of 65 [32%] in the nonbiopsied cohort, $P = 0.0003$).

Interestingly, zero crossing count was shown to be a poor measure of morphologic irregularity overall because of its inability to distinguish the largest from the smallest tumors (Table 4) and its negative correlations between RDAR, RDS, and entropy (Table 3). The latter was particularly surprising because an irregular contour, which would have high values for RDAR, RDS, and entropy, would be anticipated to cross its equivalent circle a greater number of times.

Discussion

Tumor morphologic or shape analysis is a promising area of research that can expand the power of CAD techniques. The current literature on the image analysis of liver tumors has

not been as extensive as that on other tumors. Shape analysis using compactness has been applied to characterize tumor progression in rat hepatomas (25) but not in human subjects. There has been preliminary development of CAD algorithms for hepatic tumors visualized on ultrasonography (26) and CT (27); however, the algorithms rely on a limited set of shape descriptors or qualitative scoring criteria to characterize the tumor shape. One recent pilot study utilized five shape descriptors to develop an image retrieval system for liver lesions (28), and another study focused on computer-aided detection of HCC tumors on CT (29); neither study attempted to evaluate the malignant potential of tumors. In fact, we are not aware of any studies examining the feasibility of applying to HCC the wide array of shape features already developed in lung and mammography CAD systems.

In this investigation, we demonstrated that the computer-aided image analysis of HCC tumors using 12 shape descriptors is technically feasible and efficient. Although the contour extraction process required manual attention, the computerized image analyses used to calculate the shape descriptors was highly efficient, requiring less than a minute to execute. The biggest strength of our algorithm is its ability to conduct multiple feature extractions for a single tumor using only a few sample points for its input. Another strength of the algorithm is its flexibility; although we programmed our algorithm to measure only 12 descriptors, it is easily customizable to measure additional shape features that have not yet been examined, including the boundary roughness (6), the convex hull depth (26), the lobulation index (8), and the spiculation index (30). Finally, while the algorithm was specifically developed to assess HCC, it has the ability to be more broadly applied to different tumors in other organ systems.

In analyzing the HCC shape, we found that no single morphologic parameter alone sufficiently describes the tumor shape. A receiver operator characteristic curve analysis (not presented) with individual shape parameters did not identify any thresholds that reliably distinguished "regular" from "irregular" (subject to definition) tumors with high sensitivity or specific-

Table 6. Comparison of AFP values, enhancement patterns, and tumor shape features between patients diagnosed via biopsy and noninvasive methods

Parameter	HCC confirmed via biopsy (n=50)	HCC diagnosed via noninvasive methods (n=68)	P
AFP			
Serum level (ng/mL)	736	52 567	0.131
Above threshold >400 ng/mL	4/50 (8%)	21/65 (32%)	0.0003
Enhancement pattern			
Typical	28/50 (56%)	52/68 (76%)	0.011
Atypical	22/50 (44%)	16/68 (24%)	0.011
Shape descriptors			
Tumor area (cm ²)	16.4±21.2	23.5±41.5	0.111
Tumor perimeter (cm)	12.8±8.1	15.3±12.1	0.084
Compactness	0.898±0.064	0.871±0.097	0.037
Mean RD	0.841±0.043	0.824±0.063	0.045
RD standard deviation	0.083±0.031	0.090±0.040	0.138
RD area ratio	0.042±0.018	0.048±0.026	0.085
Number of zero crossings	6.0±2.0	6.1±2.4	0.453
Entropy	1.41±0.13	1.43±0.18	0.251
MFD (cm)	4.00±2.54	4.69±3.51	0.108
Feret ratio	0.787±0.077	0.779±0.097	0.296
Convex hull area ratio	0.979±0.025	0.973±0.028	0.109
Convex hull perimeter ratio	0.989±0.018	0.980±0.037	0.051
Elliptic compactness	0.961±0.030	0.948±0.050	0.047
Elliptic irregularity	0.956±0.018	0.950±0.026	0.073

AFP, alpha-fetoprotein; HCC, hepatocellular carcinoma; RD, radial distance; MFD, mean Feret diameter. Data are given as mean±SD or n (%).

ity. Rather, multiple descriptors with wide dispersions together most likely provide the best capability to discriminate HCC tumors from each other. To this end, we believe some combination of the MFD, RDAR, RDS, entropy, and compactness parameters may best accomplish this task.

Our tumor shape analysis included both size-dependent and size-independent parameters. With regard to size-dependent measures, one may objectively classify tumors by size using more sophisticated two-dimensional parameters (i.e., area, perimeter, and MFD) in addition to the traditional index diameter. Interestingly, poor correlations between these three size-dependent measures and the eleven size-independent descriptors indicate that large tumor size does not automatically imply irregular tumor shape. When comparing the largest tumors as a group to smallest ones, however, the

significant morphologic differences in compactness (RDS, RDAR, CHP, and EC) suggest that these five size-independent descriptors can distinguish tumors by size, indicating that larger tumors collectively tend to be less compact, more concave, and less ellipsoid.

To validate the notion that tumor irregularity indicates aggressive growth, we showed that high AFP producing tumors demonstrated greater irregularity. Because AFP value is a proven predictor of patient survival (31) and treatment response (32, 33), this finding supports the notion that quantitative morphologic shape descriptors act as secondary indicators of tumor aggression and may provide further insight into tumor biological character. Note that in our cohort, the HCC tumors selected for biopsy tended to produce less AFP and also had more compact and rounder borders than the HCC tumors diagnosed noninvasive-

ly. This finding suggests that the HCC lesions chosen for biopsy had regular morphologic features that may have raised a lower degree of suspicion than more irregular tumors (i.e., in the non-biopsied cohort). Hence, it is plausible to surmise that gross tumor shape can influence the clinical suspicion of malignancy.

There are several limitations in our investigation. First, despite attempts to objectify the image analysis, our algorithm input is still dependent on sample points that were chosen manually. Second, one radiologist traced the tumor margins, limiting the ability to determine the effect of intra- and inter-observer bias. We attempted to reduce the potential inter-observer variability by using computerized linear interpolation to help standardize the tumor boundary coordinates. Third, undersampling a tumor boundary can distort its morphological parameters. We attempted to correct for this by selecting at least 13 points per lesion, particularly the smallest ones, while allowing up to 83 points for the largest lesions. Fourth, the extent of the tumor to the liver surface, vasculature, or other nonparenchymal tissue (e.g., gallbladder) may affect the tumor boundary through a tendency to assume the natural smoother contour of such an anatomic structure. Fifth, our algorithm focuses on external contour and ignores internal characteristics, such as hemorrhage, calcification, central scar, or gross fat, which may be features of different HCC pathological subtypes (34). Sixth, our two-dimensional shape analysis attempted to capture the representative contour of a three-dimensional (3D) object at its maximum transverse diameter. This method can become invalid for a tumor that is longer in the craniocaudal axis than in the anteroposterior axis, and morphologic analyses for multiple axial planes, or even 3D volumetry, may be necessary to accurately describe a HCC external surface. Seventh, the current study represents a descriptive investigation without extensive clinical correlations, which may be performed in future investigations.

In conclusion, computerized HCC shape analysis is feasible, and the preliminary application showed that aggressive tumors have irregular morphologies; hence, quantitative shape descriptors can improve the diagnosis

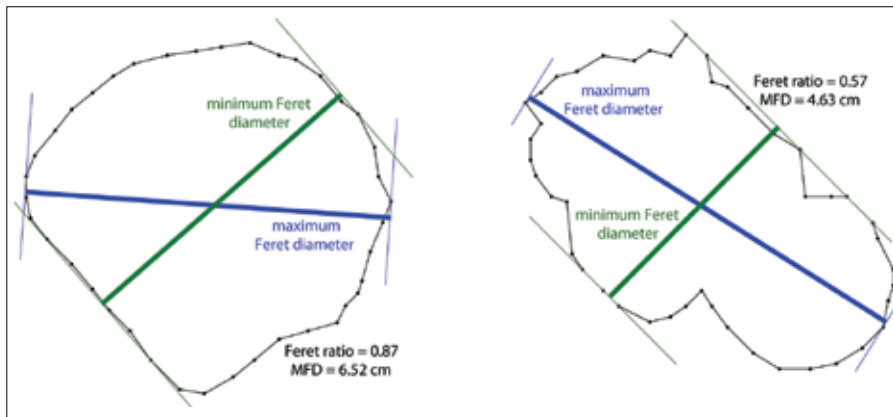


Figure 5. The maximum and minimum Feret diameters from which the Feret ratio can be calculated. MFD, mean Feret diameter.

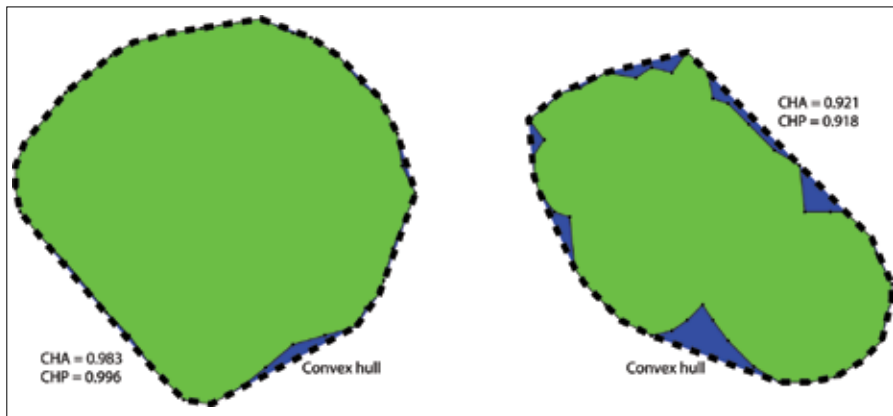


Figure 6. The tumors are enclosed by convex hulls (dashed line). The convex hull area (CHA) ratio and the convex hull perimeter (CHP) ratio can then be calculated.

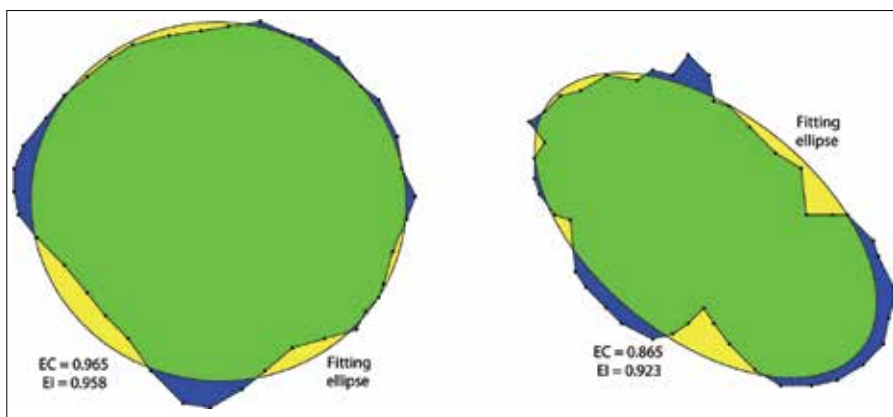


Figure 7. Tumors overlapping with their fitting ellipses. The elliptic compactness (EC) and the elliptic irregularity (EI) can then be calculated.

of HCC and may potentially help predict disease prognosis for individual patients. Further research comparing HCC tumor shapes with benign liver lesions and correlating shape descriptors with tumor histology, therapeutic agent uptake, treatment response, and overall clinical outcome should be conducted to evaluate the efficacy

and potential of applying morphologic analysis to HCC. The inclusion of morphologic imaging analysis has the potential to improve our understanding of the radiologic-pathologic correlations of HCC as well as the relevant imaging features of post-treatment imaging. We believe our shape analysis algorithm opens a new avenue for

radiologists to accomplish this challenging task and moves imagers a step closer to the implementation of a CAD system for liver lesions.

Conflict of interest disclosure

The authors declared no conflicts of interest.

Appendix is available in the online version of this article at http://www.dirjournal.org/summary_en_doi.php?doi=10.4261/1305-3825.DIR.5973-12.1

References

1. Pektas ZO, Keskin A, Gunhan O, Karslioglu Y. Evaluation of nuclear morphometry and DNA ploidy status for detection of malignant and premalignant oral lesions: quantitative cytologic assessment and review of methods for cytomorphometric measurements. *J Oral Maxillofac Surg* 2006; 64:628–635. [CrossRef]
2. Mogilner JG, Eldar S, Sabo E, et al. Computer-assisted image analysis can aid the prognostication of advanced-stage neuroblastomas. *J Cancer Res Clin Oncol* 2000; 126:285–290. [CrossRef]
3. Delahunt B, Sika-Paotonu D, Bethwaite PB, et al. Fuhrman grading is not appropriate for chromophobe renal cell carcinoma. *Am J Surg Pathol* 2007; 31:957–960. [CrossRef]
4. American College of Radiology. BI-RADS Committee. *ACR BI-RADS breast imaging and reporting data system: breast imaging atlas*. 4th ed. Reston, VA: American College of Radiology; 2003.
5. Erasmus JJ, Connolly JE, McAdams HP, Roggli VL. Solitary pulmonary nodules: Part I. Morphologic evaluation for differentiation of benign and malignant lesions. *Radiographics* 2000; 20:43–58.
6. Kilday J, Palmieri F, Fox MD. Classifying mammographic lesions using computerized image analysis. *IEEE Trans Med Imaging* 1993; 12:664–669. [CrossRef]
7. Iwano S, Nakamura T, Kamioka Y, Ikeda M, Ishigaki T. Computer-aided differentiation of malignant from benign solitary pulmonary nodules imaged by high-resolution CT. *Comput Med Imaging Graph* 2008; 32:416–422. [CrossRef]
8. Chen CM, Chou YH, Han KC, et al. Breast lesions on sonograms: computer-aided diagnosis with nearly setting-independent features and artificial neural networks. *Radiology* 2003; 226:504–514. [CrossRef]
9. Savelonas M, Maroulis D, Sangriotis M. A computer-aided system for malignancy risk assessment of nodules in thyroid US images based on boundary features. *Comput Methods Programs Biomed* 2009; 96:25–32. [CrossRef]
10. Chen CY, Chiou HJ, Chou SY, et al. Computer-aided diagnosis of soft-tissue tumors using sonographic morphologic and texture features. *Acad Radiol* 2009; 16:1531–1538. [CrossRef]

11. Raoul JL. Natural history of hepatocellular carcinoma and current treatment options. *Semin Nucl Med* 2008; 38:13–18. [\[CrossRef\]](#)
12. Altekruse SF, McGlynn KA, Reichman ME. Hepatocellular carcinoma incidence, mortality, and survival trends in the United States from 1975 to 2005. *J Clin Oncol* 2009; 27:1485–1491. [\[CrossRef\]](#)
13. El-Serag HB, Rudolph KL. Hepatocellular carcinoma: epidemiology and molecular carcinogenesis. *Gastroenterology* 2007; 132:2557–2576. [\[CrossRef\]](#)
14. Di Bisceglie AM. Epidemiology and clinical presentation of hepatocellular carcinoma. *J Vasc Interv Radiol* 2002; 13:169–171. [\[CrossRef\]](#)
15. Kim KE, Park MS, Bentley-Hibbert S, et al. Hepatocellular carcinoma: clinical and radiological findings in patients with chronic B viral hepatitis and chronic C viral hepatitis. *Abdom Imaging* 2012; 37:591–594. [\[CrossRef\]](#)
16. Minematsu S, Tani T. Clinicopathological evaluation of angiograms in hepatocellular carcinoma. *Nihon Geka Gakkai Zasshi* 1988; 89:1028–1039.
17. Lim JH, Jang HJ, Kim EY, Park CK, Joh JW, Kim YI. Early recurring hepatocellular carcinoma after partial hepatic resection: preoperative CT findings. *Korean J Radiol* 2000; 1:38–42. [\[CrossRef\]](#)
18. Iguchi T, Aishima S, Taketomi A, et al. Extracapsular penetration is a new prognostic factor in human hepatocellular carcinoma. *Am J Surg Pathol* 2008; 32:1675–1682. [\[CrossRef\]](#)
19. Huppert PE, Lauchart W, Duda SH, et al. Chemoembolization of hepatocellular carcinomas: which factors determine therapeutic response and survival? *Rofo* 2004; 176:375–385.
20. Kim H, Park MS, Choi JY, et al. Can microvessel invasion of hepatocellular carcinoma be predicted by pre-operative MRI? *Eur Radiol* 2009; 19:1744–1751. [\[CrossRef\]](#)
21. Ikenaga N, Chijiwa K, Otani K, Ohuchida J, Uchiyama S, Kondo K. Clinicopathologic characteristics of hepatocellular carcinoma with bile duct invasion. *J Gastrointest Surg* 2009; 13:492–497. [\[CrossRef\]](#)
22. Bruix J, Sherman M, Llovet JM, et al. Clinical management of hepatocellular carcinoma. Conclusions of the Barcelona-2000 EASL conference. European Association for the Study of the Liver. *J Hepatol* 2001; 35:421–430. [\[CrossRef\]](#)
23. Riaz A, Miller FH, Kulik LM, et al. Imaging response in the primary index lesion and clinical outcomes following transarterial locoregional therapy for hepatocellular carcinoma. *JAMA* 2010; 303:1062–1069. [\[CrossRef\]](#)
24. McNitt-Gray MF, Hart EM, Wyckoff N, Sayre JW, Goldin JG, Aberle DR. A pattern classification approach to characterizing solitary pulmonary nodules imaged on high resolution CT: preliminary results. *Med Phys* 1999; 26:880–888. [\[CrossRef\]](#)
25. Spillman WB Jr, Robertson JL, Meissner KE, et al. Shape factor analysis of progressive rat hepatoma images. *J Biomed Opt* 2008; 13:014030. [\[CrossRef\]](#)
26. Kim SH, Lee JM, Kim KG, et al. Computer-aided image analysis of focal hepatic lesions in ultrasonography: preliminary results. *Abdom Imaging* 2009; 34:183–191. [\[CrossRef\]](#)
27. Matake K, Yoshimitsu K, Kumazawa S, et al. Usefulness of artificial neural network for differential diagnosis of hepatic masses on CT images. *Acad Radiol* 2006; 13:951–962. [\[CrossRef\]](#)
28. Xu J, Faruque J, Beaulieu CF, Rubin D, Napel S. A comprehensive descriptor of shape: method and application to content-based retrieval of similar appearing lesions in medical images. *J Digit Imaging* 2012; 25:121–128. [\[CrossRef\]](#)
29. Xu J-W, Suzuki K, Hori M, Oto A, Baron R. Computer-aided detection of hepatocellular carcinoma in multiphase contrast-enhanced hepatic CT: a preliminary study. *Medical Imaging* 2011; 7963:79630S
30. Rangayyan RM, Mudigonda NR, Desautels JE. Boundary modelling and shape analysis methods for classification of mammographic masses. *Med Biol Eng Comput* 2000; 38:487–496. [\[CrossRef\]](#)
31. Nomura F, Ohnishi K, Tanabe Y. Clinical features and prognosis of hepatocellular carcinoma with reference to serum alpha-fetoprotein levels. Analysis of 606 patients. *Cancer* 1989; 64:1700–1707. [\[CrossRef\]](#)
32. Shao YY, Lin ZZ, Hsu C, Shen YC, Hsu CH, Cheng AL. Early alpha-fetoprotein response predicts treatment efficacy of antiangiogenic systemic therapy in patients with advanced hepatocellular carcinoma. *Cancer* 2010; 116:4590–4596. [\[CrossRef\]](#)
33. Hu HT, Kim JH, Lee LS, et al. Chemoembolization for hepatocellular carcinoma: multivariate analysis of predicting factors for tumor response and survival in a 362-patient cohort. *J Vasc Interv Radiol* 2011; 22:917–923. [\[CrossRef\]](#)
34. Chung YE, Park MS, Park YN, et al. Hepatocellular carcinoma variants: radiologic-pathologic correlation. *AJR Am J Roentgenol* 2009; 193:7–13. [\[CrossRef\]](#)
35. Zunic J, Rosin PL. A new convexity measure for polygons. *IEEE Trans Pattern Anal Mach Intell* 2004; 26:923–934. [\[CrossRef\]](#)
36. Fitzgibbon AW, Pilu M, Fisher RB. Direct Least Squares Fitting of Ellipses. *IEEE Transactions on Pattern Analysis and Machine Intelligence* 1999; 21:476–480. [\[CrossRef\]](#)